

# Formation of defects in cubic GaN grown on nano-patterned 3C-SiC (001)

R. M. Kemper<sup>\*1</sup>, M. Häberlen<sup>1</sup>, T. Schupp<sup>1</sup>, M. Weini<sup>1</sup>, M. Bürger<sup>1</sup>, M. Ruth<sup>1</sup>, C. Meier<sup>1</sup>, T. Niendorf<sup>2</sup>, H. J. Maier<sup>2</sup>, K. Lischka<sup>1</sup>, D. J. As<sup>1</sup>, and J. K. N. Lindner<sup>1</sup>

<sup>1</sup> University of Paderborn, Department of Physics, Warburger Str. 100, 33098 Paderborn, Germany

<sup>2</sup> University of Paderborn, Lehrstuhl für Werkstoffkunde, Pohlweg 47-49, 33098 Paderborn, Germany

Received 19 May 2011, accepted 16 January 2012

Published online 17 February 2012

**Keywords** nitrides, molecular beam epitaxy, nanostructures, defects

\* Corresponding author: e-mail rkemper@mail.uni-paderborn.de, Phone: +49 (0)5251 60-5830, Fax: +49 (0)5251 60-5843

We report an anisotropic formation of defects in cubic GaN grown on nano-patterned 3C-SiC/Si (001) by molecular beam epitaxy. Nano-patterning of 3C-SiC/Si (001) is achieved by nanosphere lithography and a reactive ion etching process. Atomic force microscopy and scanning electron microscopy show that the selective-area-grown cubic GaN nucleates in two structurally different domains, which most probably originate from the

substrate. In adjacent domains the formation of defects, especially hexagonal inclusions, is different and leads to two different surface morphologies. The dominant phase within these domains was measured by electron backscatter diffraction. Optical properties were investigated by micro-photoluminescence and cathodoluminescence spectroscopy.

© 2012 WILEY-VCH Verlag GmbH & Co. KGaA, Weinheim

**1 Introduction** GaN is the material enabling a variety of highly efficient optoelectronic, high-frequency and high-power devices [1-3]. In its thermodynamically stable wurtzite phase, spontaneous and piezoelectric polarization along the c-axis can lead to performance degrading effects, like the quantum confined Stark effect decreasing the quantum efficiency of GaN based LEDs.

In contrast to hexagonal GaN, cubic GaN is free of spontaneous polarization due to its non-polar nature. Despite recent success in the improvement of structural quality, defect densities are still large and cause leakage currents in devices based on cubic GaN [4]. A fundamental defect formation mechanism in the growth of cubic GaN is the change of the stacking sequence of {111} planes.

Recently it has been shown that one way to reduce the defect density in thin cubic GaN layers is to use nano-patterned 3C-SiC/Si (001) substrates [5]. These films exhibit a preferential orientation of stacking fault (SF) type defects on the (-11-1) plane, the origin of which is not clear yet. In order to study the defect formation in molecular beam epitaxy (MBE) grown cubic GaN, in the present paper the layer thickness is increased above typical values at which high-quality cubic GaN would be achieved in or-

der to enhance the probability for stacking fault and hexagonal phase formation. This makes it easier to investigate the anisotropy in defect formation. The results presented here allow for the discussion of the effect of substrate patterning on extended defect formation in MBE grown cubic GaN, potentially enabling a more efficient defect reduction via optimized nano-epitaxy.

**2 Experimental** Cubic GaN was grown by plasma-assisted MBE on nano-patterned 3C-SiC/Si (001). The used substrates consist of 12 μm thick 3C-SiC (001) films on top of 500 μm Si [6]. Substrate patterning was achieved by nanosphere lithography as described in [7]. This method - in combination with an additional reactive ion etching process - allows the creation of cylindrical holes in 3C-SiC, which are arranged in a hexagonally closed packed array [5]. Holes have a diameter of ~500 nm with a smallest distance between them of 70-90 nm and a depth of 400 nm.

On this nano-patterned 3C-SiC/Si (001) substrate a 1.4 μm-thick cubic GaN (001) film was grown by MBE. The growth process was performed under 1 ML Ga coverage of the surface [8] and at a growth temperature of 750 °C. Reflection high energy electron diffraction was used for in-

situ monitoring of the sample surface. For comparison a reference sample with a planar cubic GaN layer was grown on an unstructured substrate. The large layer thickness was chosen to achieve a pronounced lateral growth and to encourage the formation of facets. It should be noted that in comparison to other growth processes like MOVPE, the lateral growth rate in MBE is small. After growth, the surface morphology, the structural and the optical properties of the selective-area-grown cubic GaN were investigated by scanning electron microscopy (SEM), atomic force microscopy (AFM), high-resolution X-ray diffraction (HRXRD), electron backscatter diffraction (EBSD), microphotoluminescence ( $\mu$ -PL) and cathodoluminescence (CL), respectively.

### 3 Results and discussion

**3.1 Scanning electron and atomic force microscopy** Figure 1(a) shows a top view SEM image of the surface of cubic GaN layer grown on nano-patterned 3C-SiC/Si(001). Even though the film thickness is as large as 1.4  $\mu\text{m}$  the GaN film is still discontinuous and exhibits a close packed array of residual holes. Different domains showing different secondary electron yield can be clearly distinguished. These domains have an arbitrary shape with lateral dimensions varying from a few microns up to about 100  $\mu\text{m}$ . In addition different surface morphologies are observed in the two domains in the detail SEM image of Fig. 1(b). Furthermore a close inspection of domain 1 reveals that irregularities in the periodic nanopattern on the substrate do not influence the domain structure or surface morphology of GaN. This is an indication that the different morphologies originate from the substrate. The reason for these different GaN growth types is assumed to be either differently oriented SiC grains in the substrate or differently terminated surface steps on the SiC, leading to different polarities of GaN and different growth behaviour.

Figure 2 shows an AFM image of two adjacent domains on the surface of GaN grown on the prepatterned substrate. In domain 1 GaN grows with atomically smooth facets, indicating that in this region the Frank-Van-der-Merwe growth mechanism dominates. Due to the lateral growth the shape of the nanostructures changes from circular holes before GaN growth into triangle-shaped ones afterwards. The diameter of the holes is reduced from 500 nm before GaN growth to 100–200 nm after growth. In contrast to the layer-by-layer growth mechanism in domain 1, cubic GaN seems to grow in form of islands in domain 2 (Fig. 2). The shape of the holes after GaN growth has changed into squares with diameters from 200 to 350 nm. Also the lateral growth exhibits anisotropic behavior in the different domains.

**3.2 High-resolution X-ray diffraction** The structural quality, averaged over all domains of the patterned cubic GaN film, is investigated by HRXRD measurements. Figure 3 shows a symmetrical reciprocal space map around the (002) reflection of GaN. The FWHM of the rocking

curve of the selective-area-grown cubic GaN is about 25 arcmin. An amount of 78% hexagonal inclusions in the selective-area-grown cubic GaN is estimated from the height of cubic GaN (002) and hexagonal (-1011) spots. The amount of hexagonal inclusions is very high as

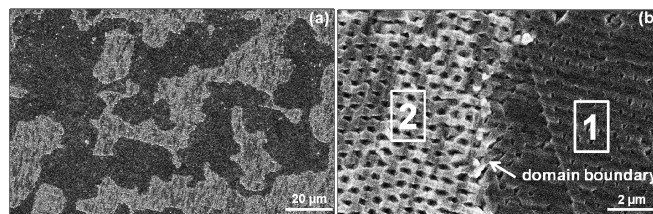


**Figure 1** (a) Top view SEM image of the surface of 1.4  $\mu\text{m}$  thick cubic GaN layer grown on nano-patterned 3C-SiC/Si(001). (b) Enlarged section of (a) showing the different size and orientation of residual holes in the two domains (1 and 2).

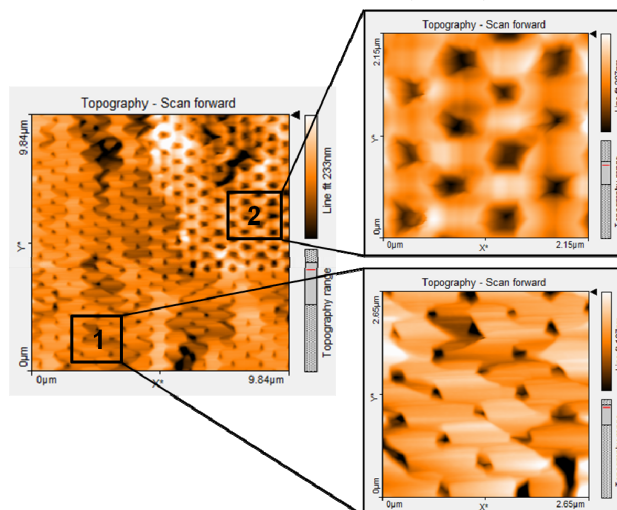


**Figure 2** AFM image of the surface of the selective-area-grown cubic GaN with two adjacent domains. Zoom-in sections on the right show a step-flow-like flat surface in domain 1 and a more three-dimensional surface morphology in domain 2.

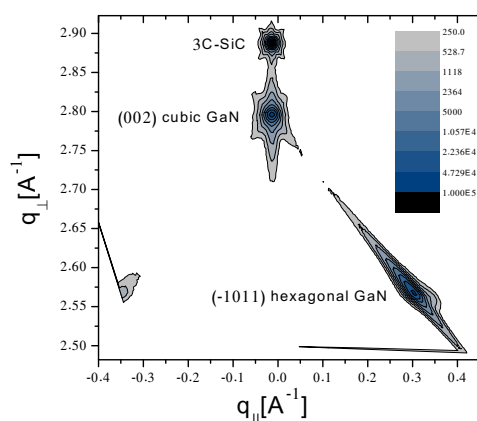


**Figure 3** A symmetrical reciprocal space map around the (002) reflection of the selective-area-grown GaN.

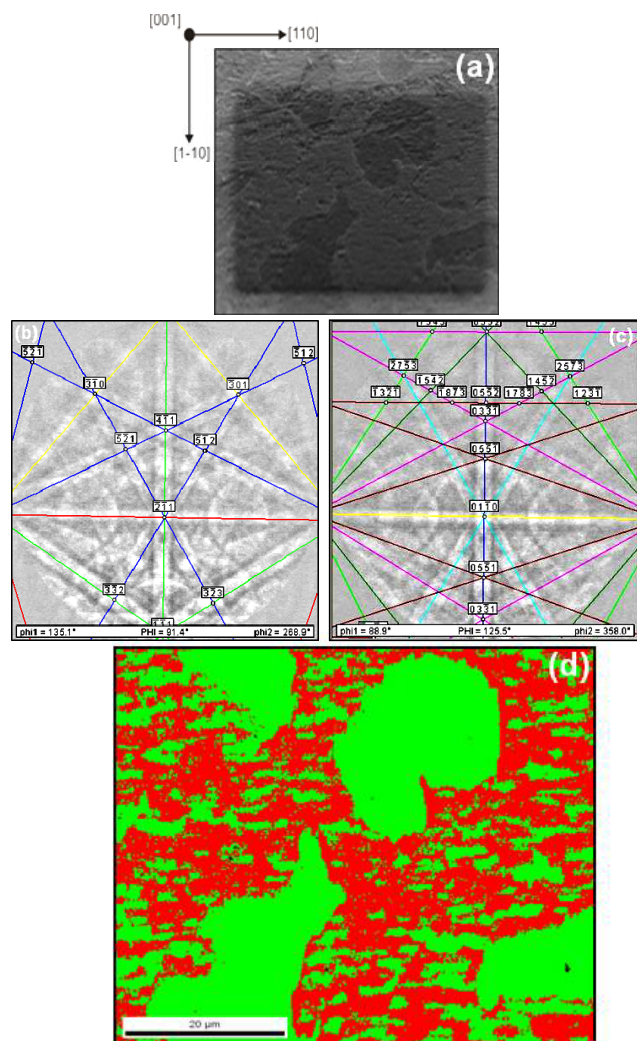


**Figure 4** (a) Top view SEM image of the EBSD-measurement area on the surface of the selective-area-grown cubic GaN sample, which is tilted to about 70° in the measurement setup, (b) diffraction pattern of the cubic phase and (c) hexagonal phase of GaN together with indexed Kikuchi lines. (d) Phase map showing regions of predominantly cubic (red) and hexagonal (green) GaN.

compared to the cubic GaN reference layer (17% hexagonal inclusions and 21 arcmin FWHM of the (002) rocking curve, not shown). However, the quality of the cubic phase of the selective-area-grown GaN and the reference layer are identical. Former studies have shown that thin cubic GaN layers (400 nm) grown on pre-patterned 3C-SiC/Si (001) have a negligible amount of hexagonal inclusions [5]. It seems that substrate patterning enhances the formation of hexagonal inclusions, which become clearly noticeable in thick layers. This could be due to {111} facets at the nanostructure sidewalls where the growth of the stable hexagonal phase is supported.

**3.3 Electron backscatter diffraction** EBSD measurements were used for phase identification of the se-

lective-area-grown GaN domains. For this method the primary electron beam (20 kV) of a tungsten cathode of a XL40 ESEM is inelastically and elastically scattered by the crystal planes of the sample. This yields Kikuchi diffraction patterns, in which each pair of Kikuchi lines represents a crystal plane [9]. Figure 4(a) shows a top view SEM image of the EBSD-measurement area on the surface of the selective-area-grown cubic GaN sample, which is tilted to about 70° in the microscope. The domains described above are also seen in this image. The diffraction pattern of the cubic (Fig. 4(b)) and the hexagonal phase (Fig. 4(c)) of GaN exemplify the measured raw data and lead to the phase map in Fig. 4(d). The crystal plane identification was achieved by a Hough-transformation followed by a least-square fit to both the cubic and the hexagonal phase, yielding a phase identification based on the smallest error. The raw data illustrated in the phase map were detected with a stepsize of 0.6 μm and an angle resolution of 1-2°. The cubic phase is displayed in red color and the hexagonal phase of GaN in green, where a 50 % threshold is used to assign either phase to a measurement position. I.e., even though it is assumed that both phases are present in the domains, a sharp discrimination of the two pure phases is made in this diagram, and it obviously strongly correlates with the SEM image in Fig. 4(a). It is clearly visible that the fraction of hexagonal phase between close-by domains varies. The domains with mainly cubic phase (red) contain hexagonal inclusions (green). Additionally there are domains where the hexagonal phase (green) dominates. These domains are less charged (darker) in the SEM image of Fig. 4(a). The correlation between SEM images and AFM measurements demonstrates that in domains with island growth the cubic phase is dominant. Furthermore the domains with a layer-by-layer growth mechanism can be identified to contain a high fraction of the hexagonal phase.

**3.4 Micro-photoluminescence and cathodoluminescence spectroscopy**

The optical properties of the domains of the selective-area-grown GaN layer were studied by room temperature μ-PL and CL measurements. In the inset of Fig. 5 a top view SEM image of the μ-PL and CL measurement area on the sample surface is displayed. Each domain is identified with contamination markers (dark rectangles) deposited by a SEM. Position 1 (blue) is allocated to a domain with a Frank-Van-der-Merwe growth mechanism, while position 2 (red) marks a domain with a Volmer-Weber island growth. The spot diameters of both optical methods are smaller than the domain size.

The μ-PL luminescence was excited by the 325 nm line of a HeCd laser with a power of 5 mW (beam diameter 1 μm). In Fig. 5 the spectra of two domains (position 1 blue curve and position 2 red curve, solid line) of the selective-area-grown cubic GaN are depicted. The band-edge luminescence of position 1 (blue curve) is at 3.38 eV and is assigned to defect luminescence related to the hexagonal phase. It should be noted that a pure hexagonal phase is

expected to show a luminescence peak at 3.42 eV, which would be clearly separated from the peak observed here. By comparison, the  $\mu$ -PL peak of domain 2 has more intensity and occurs at 3.20 eV. This value agrees well with the band-edge transition at 3.21 eV for cubic GaN grown on GaAs [10]. Furthermore there is an emission shoulder with low intensity at 3.38 eV, which is an indication for defects and hexagonal inclusions in the selective-area-grown cubic GaN. A further luminescence peak in the red curve at 2.23 eV is related to defect luminescence. These spectra demonstrate clearly that in addition to the structural differences shown by EBSD the optical properties between two adjacent domains are quite different.

To support the  $\mu$ -PL measurements and to obtain more spatially-resolved information about the optical properties of domains, CL measurements were performed in a ZEISS DSM 950 SEM equipped with an Oxford Instruments CL302. The beam energy and diameter of the excitation volume were 5 keV and  $\sim 300$  nm, respectively. Figure 5 displays the CL spectra of position 1 and position 2 (intensity is multiplied by 100) as dashed lines. Both peaks at 3.38 eV (domain 1) and 3.21 eV (domain 2) agree well with the experimental results of the  $\mu$ -PL measurements.

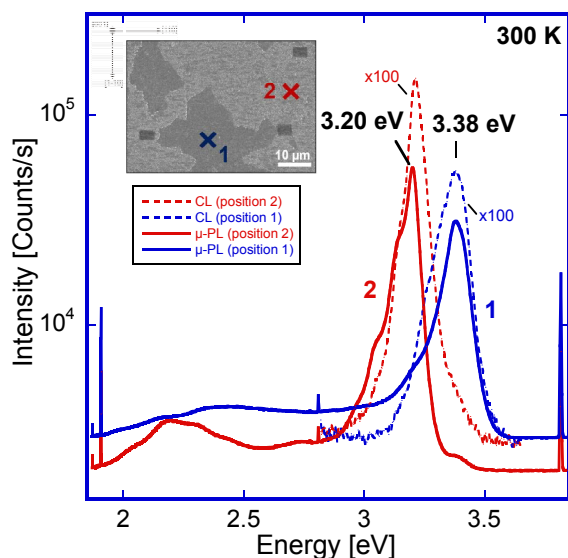


**Figure 5**  $\mu$ -Photoluminescence spectra (solid lines) and cathodoluminescence spectra (dashed lines, intensity multiplied by 100) of adjacent domains (position 1 blue curve and position 2 red curve) of the selective-area-grown cubic GaN at room temperature. Inset: Top view SEM image of the  $\mu$ -PL and CL measurement area on the sample surface. Each domain is identified with markers (dark rectangles) positioned by a SEM. Position 1 is allocated to a domain with a smooth Frank-Van-der-Merwe growth mechanism, while position 2 marks a domain with island growth.

**4 Conclusions** Using SEM and AFM measurements it is demonstrated that selective-area-grown cubic GaN grows on SiC/Si (001) in two different domains. Nano-patterning of the substrate does not influence the shape of these do-

main, which most probably originate from the substrate. It is likely that the domains are due to the presence of two different sets of  $\{111\}$  planes in cubic GaN, which are either Ga- or N-terminated and which in metal organic chemical vapour deposition [11] were shown to have different growth behaviour. HRXRD measurements show that at large layer thicknesses the hexagonal fraction in selective-area-grown cubic GaN is strongly enhanced. Several independent measurement techniques reveal that there is a largely differing amount of hexagonal inclusions and defects in the two sets of domains. Depending on the fraction of cubic or hexagonal phase the Volmer-Weber or the Frank-Van-der-Merwe growth mechanism dominates and the lateral growth rate varies accordingly. These observations need to be considered carefully in order to further reduce SF densities and hexagonal phase content in MBE grown selective-area-grown cubic GaN layers.

**Acknowledgements** The authors would like to thank Prof. Dr W. Bremser and especially Dipl.-Chem. Ing. N. Buitkamp (University of Paderborn) for access to the SEM. The work at Paderborn was financially supported by German Science Foundation (DFG).

## References

- [1] S. Nakamura, I. Mukai, and M. Senok, *Appl. Phys. Lett.* **64**, 1687 (1994).
- [2] S. Rajan, P. Waltereit, C. Poblenz, S.J. Heikman, D.S. Green, J.S. Speck and U.K. Mishra, *IEEE Electron Device Lett.* **25**, 247 (2004).
- [3] H. Machhadani, M. Tchernycheva, S. Sakr, L. Rigutti, R. Colombelli, E. Warde, C. Mietze, D.J. As, and F.H. Julien, *Phys. Rev. B* **83**, 075313 (2011).
- [4] E. Tschumak, R. Granzer, J.K.N. Lindner, F. Schweiz, K. Lischka, H. Nagasawa, M. Abe, and D.J. As, *Appl. Phys. Lett.* **96**, 253501 (2010).
- [5] R.M. Kemper, M. Weinl, C. Mietze, M. Häberlen, T. Schupp, E. Tschumak, J.K.N. Lindner, K. Lischka, and D.J. As, *J. Cryst. Growth* (2011); doi:10.1016/j.jcrysgro.2010.12.042D.
- [6] T. Chassagne, A. Leycuras, C. Balloud, P. Arcade, H. Peyre, and S. Juillaguet, *Mater. Sci. Forum* **457-460**, 273 (2004).
- [7] J.K.N. Lindner, C. Seider, F. Fischer, M. Weinl, B. Stritzker, *Nucl. Instrum. Methods Phys. Res. B* **267**, 1394 (2009).
- [8] J. Schörmann, S. Potthast, D.J. As, and K. Lischka, *Appl. Phys. Lett.* **90**, 041918 (2009).
- [9] L. Reimer, *Scanning Electron Microscopy*, 2nd ed. (Springer, New York, 1998), pp. 368-374.
- [10] D.J. As, F. Schmilgus, C. Wang, B. Schöttker, D. Schikora, and K. Lischka, *Appl. Phys. Lett.* **70**, 1311 (1997).
- [11] Y. Fu, Hui Yang, D.G. Zhao, X.H. Zheng, S.F. Li, Y.P. Sun, Z.H. Feng, Y.T. Wang, and L.H. Duan, *J. Cryst. Growth* **225**, 45 (2001).